SUSY mass reconstruction methods in ATLAS

S. Laplace

SUSY Mass Reconstruction Methods in ATLAS

Sandrine Laplace
on behalf of the ATLAS collaboration

Laboratoire d'Annecy-le-Vieux de Physique des Particules LAPP,
IN2P3/CNRS, Université de Savoie

Methods to measure the sparticle masses with the ATLAS detector at the LHC are reported. The supersymmetric phenomenology is first briefly discussed in the context of the mSUGRA constrained model. Many examples of recent studies aiming at measuring the sparticle masses are then described. Most of these examples are based on recent full simulation of the ATLAS detector.

PACS numbers: PACS numbers come here

1. Introduction

The ATLAS experiment [1] at LHC will search for Supersymmetry (SUSY), one of the most attractive extension of the Standard Model (SM) that pairs fermions and bosons to solve the hierarchy problem. The minimal R-parity conserving SUSY extension of the SM (MSSM) [1] brings 105 additional free parameters to those of the SM, thus preventing a systematic study of the full parameter space. Most of these new parameters appear during the soft breaking of SUSY and one can thus reduce their number by constraining this breaking. The mSUGRA model [2], in which the breaking is transmitted from the hidden sector to the observable sector by gravity, assumes that the gauginos and scalars masses, as well as the trilinear couplings, are unified at the GUT scale, leading to only 5 fundamental parameters: respectively $m_{1/2}$, m_0 and A_0 for the previously cited parameters, as well as $\tan\beta$, the ratio of the vacuum expectation values of the scalar fields and $sgn(\mu)$, the sign of the higgsino mass term. Constraints on mSUGRA are usually displayed in the m_0-$m_{1/2}$ plane, fixing the remaining 3 parameters to

---

[1] The MSSM contains terms that violate the baryon (B) and lepton (L) numbers conservation. The R-Parity, defined as $R = (-1)^{3(B-L)+2s}$, is a symmetry that forbids these terms.

characteristic values, as shown on Fig. 1. The measurements from WMAP, $b \to s\gamma$ and $g-2$ put strong constraints on this plane. In particular, the dark matter (thus the Lightest Supersymmetric Particle, LSP) density should be kept low according to the WMAP measurement, and the allowed regions are thus those where the LSP annihilation is large: the *bulk* at small m_0, $m_{1/2}$ values (LSP=$\tilde\chi_1^0$), where sleptons [2] are light, allows a large $\chi\chi$ annihilation by slepton exchange in the t-channel; the *stau co-annihilation* region (small m_0, LSP=$\tilde\chi_1^0$) where $m_{LSP} \simeq m_{\tilde\tau}$ allowing for a large $\tilde\tau\chi$ annihilation; the *focus point* (small $m_{1/2}$) where the LSP is mostly a Higgsino allowing a large annihilation into W and Z.
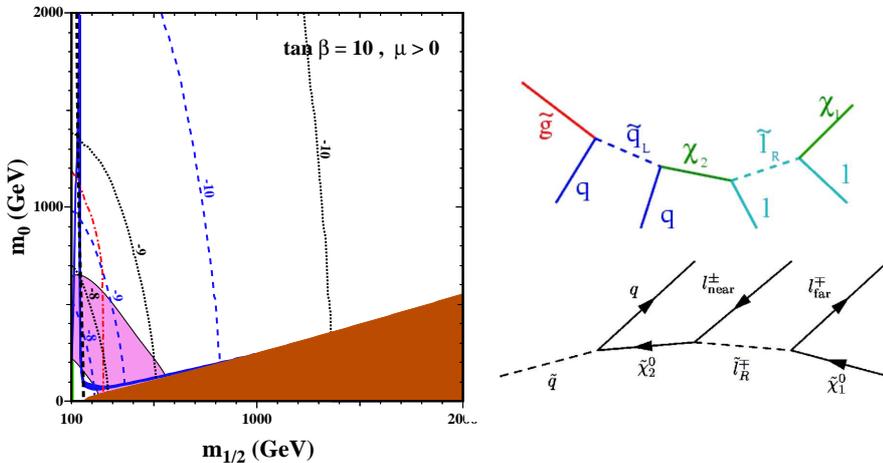

Fig. 1. <u>Left</u>: mSUGRA m_0-$m_{1/2}$ plane [3]. The orange area is theoretically excluded (the LSP is the lightest stau and is thus charged); the green area is excluded by $b \to s\gamma$; the pink area is favored by $g-2$; the blue area is favored by WMAP. The spin-independent elastic-scattering cross-sections are also shown and labeled by their exponents in units of picobarns. <u>Right</u>: generic decay chains originating from a gluino (top) or a squark (bottom).

The R-parity conservation implies that the LSP is stable. It is not detected and leads to significant missing transverse energy ($\not{E}_T$). On one hand, this provides a distinct signature for the SUSY events compared to the SM events, but on another hand this prevents the reconstruction of the full event and thus of the mass peaks. Instead, one has to exploit the kinematics of long decay chains, such as those shown on Fig. 1, originating from gluino or squark production. Note that these chains produce many

---

[2] Note that in this report, the word "sleptons" stands for selectrons and smuons. Staus are explicitly designated as such.

jets and leptons. Which route is being taken from $\tilde{g}\tilde{g}$, $\tilde{g}\tilde{q}$ or $\tilde{q}\tilde{q}$ production down to the LSP depends on which decay channels are opened and their branching ratio.

Understanding SUSY is usually done in three steps: the first step is to discover SUSY by an inclusive search; the second step is to look for particular SUSY signatures to measure the sparticle masses; the third step is to find back the fundamental model parameters from the measured masses. This report mainly concerns the second step, but the next section shortly describes the first step as well.

2. Discovering SUSY

To discriminate the SUSY signal from the SM background, one select events with at least 4 jets and large $\not{E}_T$, and constructs the variable $M_{eff} = \sum_{j=1}^{4} |p_{T,j}| + \not{E}_T$ which distribution is shown on Fig. 2 (left). For large values of M_{eff}, the signal significance is very high (*e.g.*, $S/\sqrt{B} \simeq 286$ for $M_{eff} > 1000$ GeV/c^2 with 5fb^{-1}).
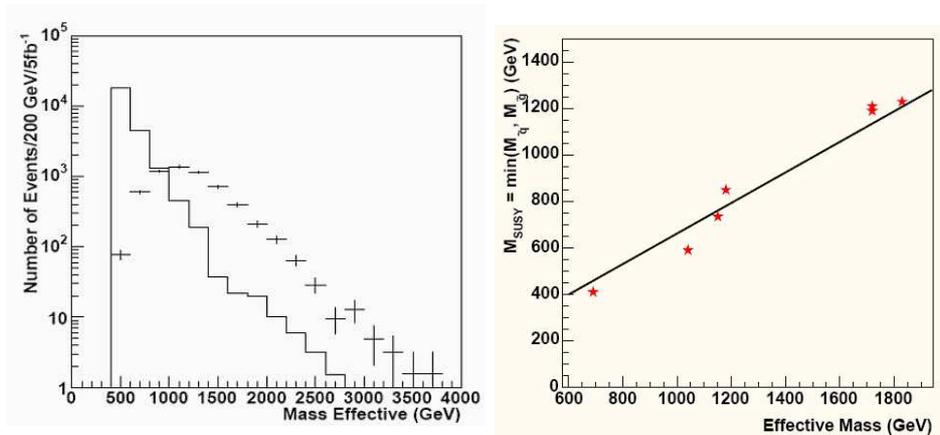

Fig. 2. <u>Left</u>: Distributions of M_{eff} for the SUSY signal (error bars) and the SM background (full line) simulated with PYTHIA (parton shower generator). The signal went through a full ATLAS simulation, but not the background. Note that simulating the background from a matrix element generator such as ALPGEN would increase it by a factor 2 to 3. <u>Right</u>: correlation between M_{eff} and m_{SUSY}.

The value of M_{eff} at which the signal exceeds the SM backgrounds provides a first estimate of the SUSY masses ($m_{SUSY} = min(m_{\tilde{g}}, m_{\tilde{q}})$) [4, 5]. as shown on Fig. 2 (right).

3. Sparticle Mass Measurement using the Endpoint Method

3.1. Looking at $\tilde{q}_L \to \tilde{\chi}_2^0 q \to \tilde{l}_R l q \to \tilde{\chi}_1^0 l l q$ (SPS1a Point)

The $\tilde{q}_L \to \tilde{\chi}_2^0 q \to \tilde{l}_R l q \to \tilde{\chi}_1^0 l l q$ decay chain (bottom-right in Fig. 1) allows to measure the masses of the $\tilde{q}_L$ [3], $\tilde{l}_R$, $\tilde{\chi}_2^0$ and $\tilde{\chi}_1^0$ sparticles. This decay chain occurs in a large region of the m_0-$m_{1/2}$ plane, in particular along the SPS1a line defined by m_0=-A_0=0.4 $m_{1/2}$, $\tan\beta$=10 and $sgn(\mu)$=+ [6].

One computes various invariant masses of the visible products in this decay chain: their endpoints correspond to particular kinematic configurations driven by the masses of the sparticles contained in the chain. Since many sparticles enter the chain, one needs to measure several endpoints in order to un-ambiguously determine the masses.

SUSY events are selected by requiring at least three energetic jets, significant $\not{E}_T$ and two isolated opposite-sign same-flavor leptons. The only SM background surviving this selection comes from $t\bar{t}$ events.

Most of the background comes from SUSY itself: the opposite-sign SUSY events have correlated (*e.g.* same flavor, SF) and uncorrelated (*e.g.* 50% SF, 50% different flavour, DF) lepton sources, the latter being dominant. The SF uncorrelated part can be subtracted using the DF events since the DF events have the same experimental characteristics than the SF events.

Figure 3 shows the dilepton (ll) and quark-lepton-lepton (qll) invariant masses for the SUSY and SM events. The endpoints are fitted from these distributions to obtain the mass differences. The statistical error is usually negligible compared to systematic error due to the lepton or jet energy scale of respectively 0.1% and 1%.

The potential of extracting the masses from the endpoint measurements is evaluated with a toy Monte-Carlo of 10000 experiments. The masses are not always un-ambiguously determined depending on which endpoints are considered. Figure 4 shows the results of this study. The obtained masses are correlated *via* the LSP mass. With 300fb^{-1}, the masses are well determined.

3.2. Di-lepton Endpoint in Co-Annihilation and Focus Points

To illustrate the dependence of the decay chain configuration on the mSUGRA point, the di-lepton endpoints are shown on figure 5 for the co-annihilation and focus points [8].

In the co-annihilation point, both the right-handed and left-handed slepton masses are lower (but close) than the $\tilde{\chi}_2^0$ mass. Therefore, both kinds

---

[3] In mSUGRA, $\tilde{\chi}_1^0$ in mostly a bino and $\tilde{\chi}_2^0$ a wino. Therefore, the dominant decay channels are $\tilde{q}_L \to q\tilde{\chi}_2^0$ and $\tilde{q}_R \to q\tilde{\chi}_1^0$: only $\tilde{q}_L$ enters the long decay chains described here, whereas $\tilde{q}_R$ decays directly to the LSP (its mass can still be measured *via* this short decay chain, though).
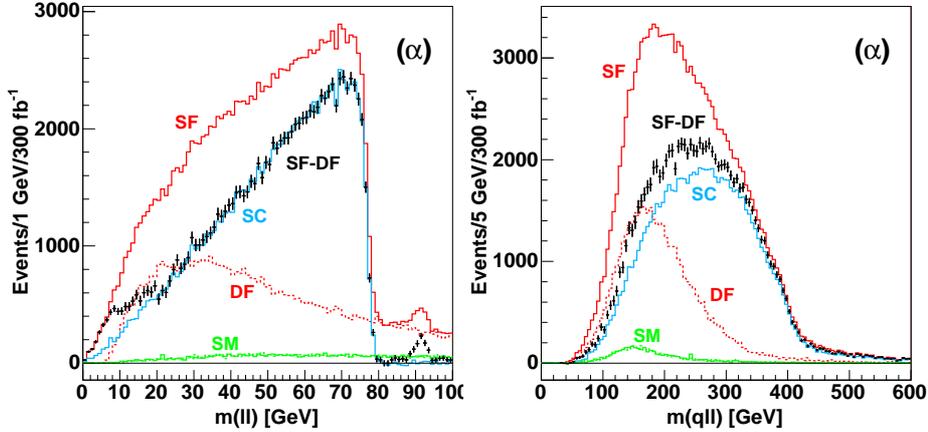
Fig. 3. Invariant mass of the dilepton (left) and quark-lepton-lepton (right) systems [6] for 300 fb^{-1} (fast simulation [7], SPS1a point). The full (resp. dashed) red curve shows the same flavor SF (resp. different flavor DF) SUSY events. After DF subtraction, one obtains the black curve which overlays with the signal chain (SC). The green curve shows the SM background.
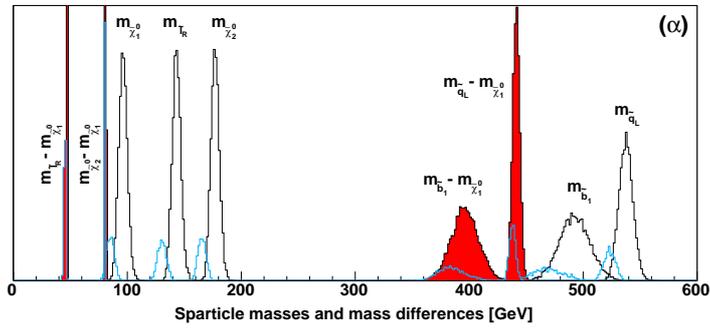

Fig. 4. Sparticle masses (empty black histograms) and mass differences (filled red histograms) for the SPS1a point. The empty blue histograms show the wrong solutions that are returned in 17% of the Monte Carlo experiments.

of sleptons are produced in the decay chain inducing two endpoints in the di-lepton invariant mass distribution.

In the focus point, m_0 is very large and thus the squarks and sfermions have masses above 2 TeV. The SUSY production is dominantly done *via* gaugino pairs but these events are hardly distinguishable from the SM. Only 10% of the SUSY production occurs *via* gluinos that decay to gauginos and jets. The gauginos decay directly to leptons. One looks at $\tilde{\chi}_3^0 \to ll\tilde{\chi}_1^0$ and $\tilde{\chi}_2^0 \to ll\tilde{\chi}_1^0$ and thus one observes two endpoints that measure the mass

difference between the heavy gauginos and the LSP.

In both analyzes, the SF-DF subtraction is used to remove the SUSY uncorrelated backgrounds. The plots show that the endpoints are well measurable already with less than 10fb^{-1}.
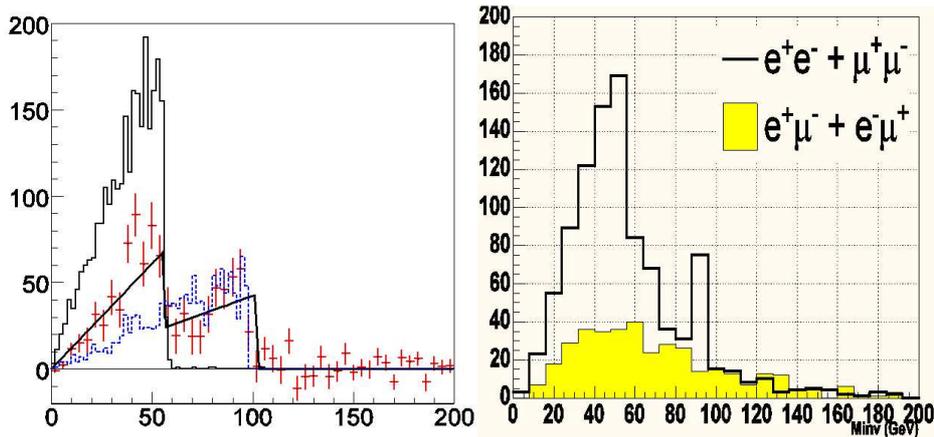

Fig. 5. <u>Left</u>: dilepton invariant mass for the co-annihilation point (full simulation, 20.6 fb^{-1}). The full dark (dashed blue) curves corresponds to the left-handed (right-handed) squark decay chains. After DF subtraction, one obtains the red curve corresponding to the signal events. <u>Right</u>: dilepton invariant mass for the focus point (full simulation, 6.9 fb^{-1}). The empty (full) histograms shows the SF and DF distributions. Apart from the Z peak, one observes two endpoints measuring $m_{\tilde{\chi}_3^0} - m_{\tilde{\chi}_1^0}$ and $m_{\tilde{\chi}_2^0} - m_{\tilde{\chi}_1^0}$.

3.3. Sbottom and Gluino Masses

Several methods are foreseen to measure the sbottom and gluino masses using gluino-initiated decay chain with the gluino decaying to $\tilde{b}b$.

The first method [9] considers the events close to the di-lepton endpoint: in this case, the LSP and the di-lepton system are almost at rest in the $\tilde{\chi}_2^0$ frame, and the $\tilde{\chi}_2^0$ momentum can be approximated by the expression: $\vec{p}_{\tilde{\chi}_2^0} \simeq \vec{p}_{ll}\sqrt{1 - m_{\tilde{\chi}_1^0}/m_{ll}}$ [4]. If the $\tilde{\chi}_1^0$ and $\tilde{\chi}_2^0$ masses are known, one can then compute the sbottom mass as $m_{\tilde{b}} = m(\tilde{\chi}_2^0 b)$ and the gluino mass as $m_{\tilde{g}} = m(\tilde{\chi}_2^0 bb)$. The correlation between these two invariant masses is shown on Fig. 6 (left): the off-diagonal events corresponds to badly associated b-jets and are thus removed. The spread of the remaining good events is

---

[4] Note that this approximation works well for the chosen point, but this would not be the case for other points where $m_{\tilde{l}_T}$ is close to either $m_{\tilde{\chi}_2^0}$ or $m_{\tilde{\chi}_1^0}$.

due to the $\tilde{\chi}_2^0$ momentum approximation. The gluino mass can be precisely measured with 300 fb^{-1} as shown on Fig. 6 (right).
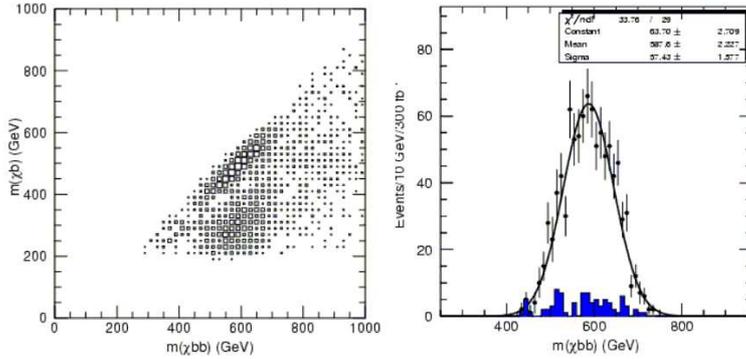

Fig. 6. <u>Left</u>: Correlation between $m(\tilde{\chi}_2^0 b)$ and $m(\tilde{\chi}_2^0 bb)$. The off-diagonal events correspond to badly associated b-jets. <u>Right</u>: Gluino mass given by $m(\tilde{\chi}_2^0 bb)$ for 300fb^{-1}, fast simulation.

Figure 7 (left) shows the difference $m(\tilde{\chi}_2^0 bb) - m(\tilde{\chi}_2^0 b)$ in which the spread due to the $\tilde{\chi}_2^0$ momentum approximation is factored out. The two states $\tilde{b}_1$ and $\tilde{b}_2$ are not well separated but can still be distinguished with a large luminosity (300 fb^{-1}).

The second method [10], called the Mass Reconstruction Method, makes use of all the events. The idea is to completely solve the kinematics of the SUSY cascade decay by using the assumption that the selected events satisfy the same mass shell conditions of the sparticles involved in the cascade decay. Knowing the $\tilde{\chi}_1^0$, $\tilde{l}_R$ and $\tilde{\chi}_2^0$ masses, one can determine the gluino and sbottom mass and discriminate the two sbottom states.
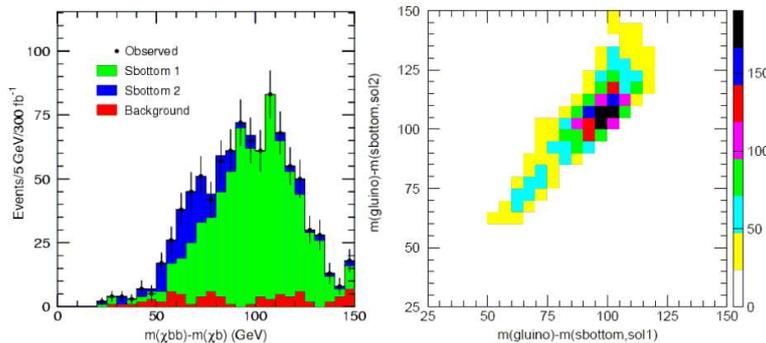

Fig. 7. <u>Left</u>: Sbottom mass given by $m(\tilde{\chi}_2^0 b)$. The two states of the sbottom quarks are distinguishable with 300 fb^{-1}. <u>Right</u>: The two solutions of the Mass Reconstruction Method. The two sbottom peaks are well separated.

A third method makes use of additional endpoints using the quark from the gluino decay into $\tilde{l}_L$. It is not described here, see [11] for more details.

3.4. Conclusion

At a few months of the LHC startup, a new era has started in the ATLAS experiment: a large scale production of Monte Carlo events using the full detector simulation is currently being analyzed. Systematic errors are being more precisely inferred and methods are being developed to evaluate the backgrounds more precisely. Also, new models and new analysis techniques are being investigated. In most models, a few fb^{-1} are sufficient to observe squarks and gluinos up to a mass of 1 or 2 TeV/c^2 and sleptons up to 300 GeV/c^2 and to precisely measure their mass using cascade decays.

Acknowledgments

REFERENCES

[1] ATLAS Collaboration, ATLAS TDR, CERN/LHCC/99-14, http://atlasinfo.cern.ch/ Atlas/GROUPS/PHYSICS/TDR/access.html.

[2] L. Alvarez-Gaume, J. Polchinski et M. B. Wise, *Nucl. Phys.* B **221**, 495 (1983); L. Ibanez, *Phys. Lett.* B **118**, 73 (1982); J. Ellis, D. V. Nanopoulos et K. Tamvakis,

[3] J. R. Ellis, K. A. Olive, Y. Santoso and V. C. Spanos, Phys. Rev. D **71** (2005) 095007

[4] I. Hinchliffe, F. E. Paige, M. D. Shapiro, J. Soderqvist and W. Yao, Phys. Rev. D **55** (1997) 5520

[5] D. R. Tovey, Phys. Lett. B **498** (2001) 1

[6] B. K. Gjelsten, D. J. Miller and P. Osland, JHEP **0412** (2004) 003

[7] E. Richter-Was, D. Froidevaux and L. Poggioli, ATLFAST 2.0: A fast simulation Package for ATLAS, ATL-PHYS-98-131 (1998)

[8] I. Borjanovic [ATLAS Collaboration],PoS **HEP2005** (2006) 350

[9] B. K. Gjelsten, D. J. Miller, P. Osland and G. Polesello, G ATL-PHYS-2004-007

[10] K. Kawagoe, M. M. Nojiri and G. Polesello, Phys. Rev. D **71** (2005) 035008

[11] B. K. Gjelsten, D. J. Miller and P. Osland, JHEP **0506** (2005) 015